A new ternary derivative of the Laves phases in the Mg–Co–Ga system

Nazar Pavlyuk,[a,b]* Grygoriy Dmytriv,[a] Volodymyr Pavlyuk,[a,b] Wojciech Ciesielski,[b] Beata Rozdzynska-Kielbik,[b] Sylvio Indris[c] and Helmut Ehrenberg[c]

[a]Department of Inorganic Chemistry, Ivan Franko National University of Lviv, Kyryla and Mefodiya str. 6, 79005 Lviv, Ukraine, [b]Institute of Chemistry, Jan Długosz University in Częstochowa, al. Armii Krajowej 13/15, Częstochowa, 42200, Poland, and [c]Karlsruhe Institute of Technology (KIT), Institute for Applied Materials (IAM), Hermann-von-Helmholtz-Platz 1, D-76344 Eggenstein-Leopoldshafen, Germany. *Correspondence e-mail: nazar.pavlyuk@gmail.com

Keywords: intermetallics; Laves phases; magnesium alloys; single-crystal methods; chemical bonding.

Crystal structures of MgCoGa, $Mg_{0.74}CoGa_{0.52}$ and $Mg_{0.49}CoGa_{0.15}$ phases from the Mg–Co–Ga system were investigated using single-crystal diffraction. These structures belong to the family of so-called Laves phases. Hexagonal MgCoGa crystallizes as a disordered phase within the $MgZn_2$ structure type. The orthorhombic structure of $Mg_{0.74}CoGa_{0.52}$ is a distortion variant of $MgZn_2$ and URe_2 structure type, and the structural relation is demonstrated in terms of a Bärnighausen formalism group–subgroup transformation scheme. The structure of trigonal phase $Mg_{0.49}CoGa_{0.15}$ is strongly disordered, as is shown by the presence of adjacent atomic sites which cannot be occupied simultaneously. In $Mg_{0.49}CoGa_{0.15}$, two subcells (A and B) were obtained in a ratio of 9:1. Subcell A is closely related to $MgZn_2$-type.

1. Introduction

Laves phases have various functional applications. For example, they are known as a hydrogen storage material, as magnets or as corrosion-resistant materials *etc.* (Bououdina *et al.*, 2006; Sakintuna *et al.*, 2007; Stein & Leineweber, 2021).

The decisive factor in the formation of Laves phases is the geometric factor, namely the ratio of the atomic radii. In the parent Laves phase $MgZn_2$ r(Mg)/r(Zn) = 1.225, with an overall packing density of 0.71. In fact for different phases this ratio ranges from 1.10 to 1.60. There are three main groups of Laves phases (Lps) based on following parent types: $MgZn_2$ (hexagonal, $P6_3/mmc$, $hP12$), $MgNi_2$ (hexagonal, $P6_3/mmc$, $hP24$) and $MgCu_2$ (cubic, $Fd\bar{3}m$, $cF24$) (Laves & Witte, 1935; Komura & Tokunaga, 1980; Paufler, 2011). Among the different studied binary and ternary metallic systems, there are many known cases where these different types of Lps can be found as a single phase as a result of concentration or temperature polymorphism. For example, in the Mg–Ni–Ga system, variation of the content of Ni and Ga leads to the realization of $MgNi_{1.25}Ga_{0.75}$ ($MgCu_2$-type) and MgNiGa ($MgZn_2$-type) phases (Teslyuk & Markiv, 1962; Pavlyuk *et al.*, 2022*a*). Also, a temperature change can also cause formation of Lps of different types as a single phase. For example, in the Cd–Cu system the low-temperature modification of $CdCu_2$ phase crystallizes as the $MgZn_2$ type and the high-temperature phase forms as the $MgNi_2$ type (Massalski *et al.*, 1986; Horechyy *et al.*, 1999).

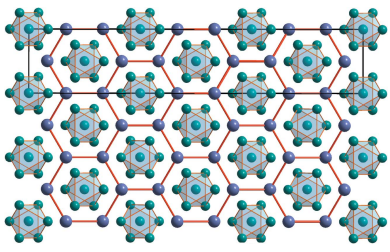

Among magnesium-containing metallic systems, Lps are most often formed in binary systems with transition metals, especially with 3*d* elements of MgT_2 composition (T = Co, Ni, Cu, Zn, *etc.*) (Komura *et al.*, 1972; Stein & Leineweber, 2021). Considering the systems with rare earth metals, where magnesium is a component with a smaller atomic radius, Lps of RMg_2 (where R = rare earth elements) composition are found. In the magnesium-based ternary systems with transition metals and *p*-block elements, mostly disordered three-component Lps are formed, as a result of structural replacement of transition metal by another *p*-block or *d*-block element (Teslyuk & Markiv, 1962; Pavlyuk *et al.*, 2022*a*). It should be noted that Lps are not formed in magnesium-based ternary systems with rare earth and transition metals. Instead, Heusler phases ($MgZn_2Ce$, $Fm\bar{3}m$, $MnCu_2Al$ structure type) or other types of phases ($(Mg_{0.137}Zn_{0.863})_{11}Ce_3$, *Immm*, $Al_{11}La_3$-type; $Mg_{2.5}Zn_{4.5}Ce$, *P*6/*mmm*, $TbCu_7$-type; $Mg_{13}Zn_{30}Ce_3$, $P6_3/mmc$, $Mg_{13}Zn_{30}Sm_3$-type; $Mg_{19}Zn_{81}Ce_{20}$, $F\bar{4}3m$, own structure type; $Mg_3Co_2Tb_4$, *P*2/*m*, $Mg_3Co_2Tb_4$-type; $MgCo_4Tb$, $F\bar{4}3m$, $MgCu_4Sn$-type; $MgCo_9Tb_2$, $R\bar{3}m$, $PuNi_3$-type) in these systems are formed (Pavlyuk *et al.*, 2007, 2012; Shtender *et al.*, 2015).

In this paper we present results of a study of the new ternary Lp phases from the Mg–Co–Ga system, carried out using single-crystal X-ray diffraction. A detailed crystallochemical analysis was carried out to reveal interrelationships with other related structures.

2. Material and methods

2.1. Synthesis of intermetallic compounds

The investigated Mg–Co–Ga samples were prepared from the pure elements: magnesium (purity is more than 99.0 wt%, Sigma-Aldrich), cobalt and gallium (purity of elements are more than 99.9 wt%, Sigma-Aldrich). Appropriate amounts of pure elements were mixed according to the target stoichiometry of the product and filled into tantalum crucibles in a glove box under an argon atmosphere. These crucibles were sealed by arc-welding in a dry argon atmosphere. The reaction between the metals was carried out for 15 min in an induction furnace heated to 1373 K. After the synthesis, tantalum crucibles were placed in evacuated quartz vials and thermally annealed to obtain single crystals of good quality for further structure determination. The heating process was carried out at a rate of 5 K min^{-1} up to T = 1073 K in a resistance furnace and this temperature was maintained for 15–20 min. Afterwards, the sample down slowly (0.1 K min^{-1}) was cooled to 673 K, and the furnace was switched off at this temperature. After cooling down to room temperature, samples were easily separated from the tantalum crucible. No side reactions of the samples with the tantalum crucibles were detected. The alloys obtained in this way are air-stable and do include single crystals, which exhibit metallic lustre and could be isolated by mechanical fragmentation.

2.2. Structure analysis and refinement

Crystal structures of MgCoGa (phase **I**), $Mg_{0.74}CoGa_{0.52}$ (phase **II**) and $Mg_{0.49}CoGa_{0.15}$ (phase **III**) were determined by means of single crystal X-ray diffraction. Single crystals were selected from slightly crushed alloys and then glued to the end of the glass capillary tubes. Crystals are stable in air. Intensities were measured using an Oxford Diffraction Xcalibur3 four-circle diffractometer (Mo $K\alpha$ radiation) equipped with a CCD detector. Unit-cell parameters were refined based on all observed reflections [$I > 2\sigma(I)$]. Scans were performed in the ω mode, the empirical absorption corrections was applied to all data (*CrysAlis Red*; Oxford Diffraction, 2008). Structures have been solved by direct methods using *SHELXS* (Sheldrick, 2008) and were refined using the *SHELXL-2014/7* program package (Sheldrick, 2015). The occupancy parameters were refined for these structures to check for deviations from the nominal compositions and the ability to form statistical mixtures.

2.3. Phase composition characterization

A TESCAN scanning electron microscope (SEM) equipped with WDS detectors was used to control the number of phases and chemical compositions of alloys. Smooth surfaces of the specimens were polished by using SiC papers and diamond pastes down to 1 μm grain diameter. The measured gross compositions were always very similar to the nominal ones from the educts. The nominal and measured compositions of the alloys, from which single crystals were selected, are reported as atomic percentages with an accuracy better than ±0.5 at.%: phase **I** ($Mg_{33.2}Co_{33.1}Ga_{33.6}$), phase **II** ($Mg_{32.6}Co_{44.2}Ga_{23.2}$), **III** ($Mg_{29.8}Co_{61.1}Ga_{9.1}$).

The density of the alloys was determined using the volumetric method. For ternary phases **I**, **II** and **III** the measured densities are 5.77 (3), 5.73 (2) and 5.87 (3) g cm^{-3}. These differences of less than 1% arise from the density calculated from single-crystal X-ray data. Since the structures are not ordered, individual positions are occupied by statistical mixtures, so it was important to compare the densities calculated from X-ray data and experimentally determined. The good consistency of these data indicates the correct refinements of the occupation of the sites in the structures.

3. Results and discussion

During the systematic study of alloys from the Mg–Co–Ga ternary system the formation of three phases in the section of 33 at.% Mg was detected. The single-crystal X-ray method was used to determine the crystal structure of these three phases in detail. The single crystal refinements give the following composition of phases for Z = 1: MgCo$_4$Ga$_4$, $Mg_{23.52}Co_{32}Ga_{16.48}$, and $Mg_{5.38}Co_{11.04}Ga_{1.59}$. In general, binary Lps have a 1:2 component ratio, for example, $MgZn_2$, $MgNi_2$ and $MgCu_2$, therefore accordingly the formulas of the Lp phases from the Mg–Co–Ga system are given as MgCoGa (for Z = 4) – phase **I**, $Mg_{0.74}CoGa_{0.52}$ (for Z = 32) – phase **II**, and $Mg_{0.49}CoGa_{0.15}$ (for Z = 11) – phase **III.**

Table 1
Experimental details.

	Phase **I**	Phase **II**	Phase **III**
Crystal data			
Chemical formula	MgCoGa	$(Mg_{0.74}CoGa_{0.52})$	$(Mg_{0.49}CoGa_{0.15})$
Structure type	$MgZn_2$	Own structure type	Own structure type
M_r (g mol^{-1})	152.9	112.70	81.45
Crystal system, space group	Hexagonal, $P6_3/mmc$	Orthorhombic, $Cmcm$	Trigonal, $R\bar{3}m$
Temperature (K)	296	293	293
a, b, c (Å)	5.0151 (5), 5.0151 (5), 8.1086 (9)	4.9868 (9), 25.959 (4), 8.0508 (11)	4.9296 (2), 4.9296 (2), 12.0744 (7)
α, β, γ (°)	90, 90, 120	90, 90, 90	90, 90, 120
V (Å^3)	176.62 (4)	1042.2 (3)	254.11 (3)
Pearson symbol, Z	$hP12$, 4	$oC72$, 32	$hR14$, 11
D_{calc} (g cm^{-3})	5.75	5.74	5.86
Z	2	32	1
Radiation type	Mo $K\alpha$	Mo $K\alpha$	Mo $K\alpha$
No. of reflections for cell measurement	177	640	97
θ range (°) for cell measurement	4.69–35.37	2.98–26.37	5.07–27.85
μ (mm^{-1})	24.40	23.12	22.04
Crystal shape	Prism	Prism	Prism
Colour	Metallic grey	Metallic grey	Metallic grey
Crystal size (mm)	0.03 × 0.02 × 0.01	0.05 × 0.04 × 0.02	0.04 × 0.03 × 0.01
Data collection			
Diffractometer	Oxford Diffraction Xcalibur3 CCD	Oxford Diffraction Xcalibur3 CCD	Oxford Diffraction Xcalibur3 CCD
Radiation source	Fine-focus sealed tube	Fine-focus sealed tube	Fine-focus sealed tube
Scan method	ω scans	ω scans	ω scans
Absorption correction	Analytical (*CrysAlis RED*)	Analytical (*CrysAlis RED*)	Analytical (*CrysAlis RED*)
T_{min}, T_{max}	0.562, 0.783	0.343, 0.630	0.457, 0.802
No. of measured, independent and observed [$I > 2\sigma(I)$] reflections	2830, 177, 172	6142, 640, 196	1136, 97, 81
R_{int}	0.047	0.093	0.070
θ_{max}, θ_{min} (°)	35.37, 4.69	26.37, 2.98	5.07, 27.85
$(\sin\theta/\lambda)_{max}$ (Å^{-1})	0.815	0.625	0.657
Refinement			
$R[F^2 > 2\sigma(F^2)]$, $wR(F^2)$, S	0.025, 0.064, 1.27	0.034, 0.089, 0.90	0.030, 0.086, 1.18
No. of reflections	177	640	97
No. of parameters	14	56	11
$\Delta\rho_{max}$, $\Delta\rho_{min}$ (e Å^{-3})	0.92, −0.92	2.36, −1.02	1.68, −1.03

Computer programs: *CrysAlis CCD* (Oxford Diffraction, 2008), *CrysAlis RED* (Oxford Diffraction, 2008), *SHELXS2014/7* (Sheldrick, 2008), *SHELXL2014/7* (Sheldrick, 2015), *DIAMOND* (Brandenburg, 2006).

Table 2
Fractional atomic coordinates and isotropic or equivalent isotropic displacement parameters (Å^2) for **I** (MgCoGa).

Atoms	Wyckoff site	x	y	z	U_{eq}	Occ. (Co/Ga)
(Co/Ga)1	6*h*	0.17012 (6)	0.34024 (11)	$\frac{1}{4}$	0.0130 (2)	0.50 (2)/0.50 (2)
(Co/Ga)2	2*a*	0	0	0	0.0153 (3)	0.50 (3)/0.50 (3)
Mg1	4*f*	$\frac{1}{3}$	$\frac{2}{3}$	0.5625 (3)	0.0126 (4)	1.0

Table 3
Atomic displacement parameters (Å^2) for phase **I** (MgCoGa).

$U^{13} = U^{23} = 0$.

Atoms	U_{11}	U_{22}	U_{33}	U_{12}
(Co/Ga)1	0.0167 (3)	0.0091 (3)	0.0106 (3)	0.00457 (15)
(Co/Ga)2	0.0190 (3)	0.0190 (3)	0.0078 (4)	0.00952 (17)
Mg1	0.0117 (5)	0.0117 (5)	0.0146 (8)	0.0058 (3)

Table 4
Geometric parameters (Å) for phase **I** (MgCoGa).

(Co/Ga)1—(Co/Ga)1	2.4556 (9)
(Co/Ga)1—(Co/Ga)2	2.5086 (3)
(Co/Ga)1—(Co/Ga)1	2.5595 (9)
(Co/Ga)2—(Co/Ga)1	2.5086 (3)
Mg1—(Co/Ga)1	2.9038 (19)
Mg1—(Co/Ga)1	2.9325 (11)

Crystal data, data collection parameters, and refinement data for phase **I** are presented in Table 1. This phase crystallizes in $MgZn_2$ structure type (hexagonal Lp). The refinement of fractional atomic coordinates, occupation, and displacement parameters shows that a cobalt and gallium atoms do form statistical mixtures in the 2*a* and 6*h* sites. The ordered magnesium atoms occupy 4*f* sites. The refined fractional atomic coordinates, displacement, and geometric parameters are presented in Tables 2, 3 and 4, respectively. The unit cell of phase **I** and coordination polyhedra for each atomic position

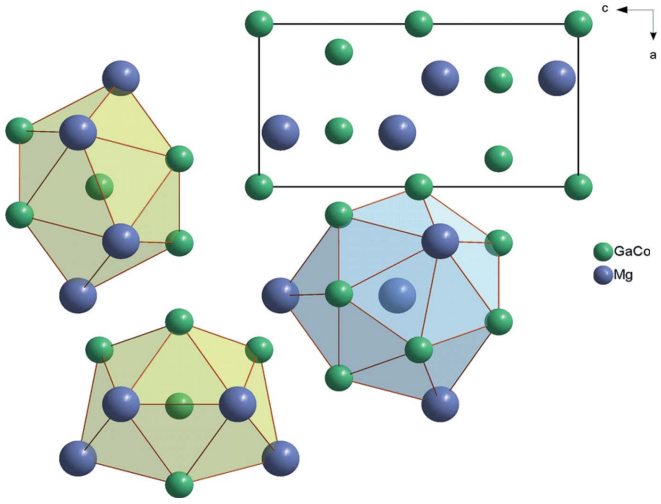

Figure 1
Phase **I** (MgCoGa) unit cell and coordination polyhedra for each atomic position.

are presented in Fig. 1. The polyhedron for Mg is a 16-vertex Frank–Kasper (FK) cage [$Mg(Co/Ga)_{12}Mg_4$]. For (Co/Ga)1 and (Co/Ga)2 with statistical atomic mixtures the coordination polyhedron is an icosahedron.

The orthorhombic phase **II** contains 72 atoms per unit cell and is closely related to Laves phases. In this phase, Mg occupies three 8*f* sites, among them two positions are fully occupied and one position emerges as a statistical mixture of 0.94Mg/0.06Ga. The possibility of replacing Mg with gallium is shown by the experimentally studied Mg–Ga phase diagram, according to which the maximum solubility of gallium in magnesium is more than 3 at.% (Okamoto, 2013). Other sites (four 4*c*, one 8*f* and three 8*g*) are occupied by different Co/Ga statistical mixtures. The refined fractional atomic coordinates, displacement and geometric parameters are presented in Tables 5, 6 and 7, respectively. The unit cell and atoms coordination polyhedra are presented in Fig. 2. The coordination polyhedra for all Mg atoms are 16-vertex FK polyhedra. For all Co/Ga statistical mixtures the coordination polyhedron is a deformed icosahedron (c.n. = 12). The Co/Ga atoms form corner- and face-sharing tetrahedra-like 3-D networks along the *z*-axis. The magnesium atoms in the *xy* plane do form 6_3-corrugated networks (Fig. 3). In the ordered hexagonal binary $MgZn_2$ and ternary Mg_2Cu_3Si Laves phases, the tetrahedra are exclusively formed by the zinc or copper atoms, respectively. In phase **II** the corner- and face-sharing tetrahedra are formed by different (Co/Ga) statistical mixtures. It is obvious that change in occupation of the tetrahedron's vertices leads to the orthorhombic distortion. A similar behaviour was also clearly observed for the previously described Mg_2MnGa_3 ternary Lp (Pavlyuk *et al.*, 2022*b*). In this Mg_2MnGa_3 phase, the composition of the tetrahedra is [$MnGa_3$].

The relation of phase **II** to original Laves phases can be given in terms of the group–subgroup scheme based on Bärnighausen form-

Table 5
Fractional atomic coordinates and isotropic or equivalent isotropic displacement parameters (Å^2) for **II** ($Mg_{0.74}CoGa_{0.52}$).

Atoms	Wyckoff site	*x*	*y*	*z*	U_{iso}*/U_{eq}	Occ. (Co/Ga)
(Co/Ga)1	4*c*	0	0.60972 (10)	$\frac{1}{4}$	0.0069 (8)	0.68 (2)/0.32 (2)
(Co/Ga)2	4*c*	0	0.94270 (11)	$\frac{1}{4}$	0.0052 (8)	0.80 (1)/0.20 (1)
(Co/Ga)3	4*c*	0	0.27584 (11)	$\frac{1}{4}$	0.0069 (7)	0.68 (1)/0.32 (2)
(Co/Ga)4	4*a*	0	0	0	0.0062 (7)	0.68 (3)/0.32 (3)
(Co/Ga)5	8*f*	0	0.33331 (8)	−0.0006 (2)	0.0074 (4)	0.70 (1)/0.30 (1)
(Co/Ga)6	8*g*	0.2570 (5)	0.02856 (7)	$\frac{1}{4}$	0.0072 (5)	0.64 (2)/0.36 (2)
(Co/Ga)7	8*g*	0.2580 (4)	0.36201 (7)	$\frac{1}{4}$	0.0075 (6)	0.62 (3)/0.38 (3)
(Co/Ga)8	8*g*	0.2429 (4)	0.19529 (7)	$\frac{1}{4}$	0.0074 (5)	0.6 (2)2/0.38 (2)
Mg1	8*f*	0	0.11103 (16)	0.0649 (8)	0.0043 (13)	1.00
Mg2	8*f*	0	0.44471 (17)	0.0654 (7)	0.0066 (13)	1.00
Mg	8*f*	0	0.22209 (17)	0.5662 (6)	0.0095 (11)*	0.94 (2)
Ga	8*f*	0	0.22209 (17)	0.5662 (6)	0.0095 (11)*	0.06 (2)

Table 6
Atomic displacement parameters (Å^2) for **II** ($Mg_{0.74}CoGa_{0.52}$).

Atoms	U_{11}	U_{22}	U_{33}	U_{12}	U_{13}	U_{23}
(Co/Ga)1	0.004 (2)	0.0113 (17)	0.0053 (17)	0.000	0.000	0.000
(Co/Ga)2	0.004 (2)	0.0069 (17)	0.0047 (15)	0.000	0.000	0.000
(Co/Ga)3	0.010 (2)	0.0055 (14)	0.0047 (16)	0.000	0.000	0.000
(Co/Ga)4	0.0069 (19)	0.0102 (15)	0.0024 (16)	0.000	0.000	0.0001 (9)
(Co/Ga)5	0.0090 (11)	0.0105 (8)	0.0026 (10)	0.000	0.000	−0.0002 (7)
(Co/Ga)6	0.0059 (13)	0.0092 (11)	0.0065 (11)	0.0009 (9)	0.000	0.000
(Co/Ga)7	0.0057 (14)	0.0099 (12)	0.0068 (12)	−0.0028 (9)	0.000	0.000
(Co/Ga)8	0.0038 (14)	0.0103 (11)	0.0080 (11)	0.0019 (10)	0.000	0.000
Mg1	0.004 (3)	0.007 (2)	0.002 (3)	0.000	0.000	0.001 (2)
Mg2	0.002 (3)	0.007 (2)	0.011 (3)	0.000	0.000	0.000 (2)

Table 7
Geometric parameters (Å) for **II** ($Mg_{0.74}CoGa_{0.52}$).

Mg1—(Co/Ga)2	2.894 (6)
Mg1—(Co/Ga)7	2.894 (6)
Mg1—(Co/Ga)1	2.905 (3)
Mg2—(Co/Ga)6	2.898 (5)
Mg2—(Co/Ga)6	2.901 (5)
Mg2—(Co/Ga)2	2.903 (3)
Mg—(Co/Ga)3	2.900 (3)
Mg—(Co/Ga)7	2.901 (5)
(Co/Ga)1—(Co/Ga)6	2.430 (3)
(Co/Ga)1—(Co/Ga)5	2.494 (3)
(Co/Ga)1—(Co/Ga)8	2.565 (3)
(Co/Ga)2—(Co/Ga)7	2.417 (3)
(Co/Ga)2—(Co/Ga)4	2.5028 (17)
(Co/Ga)2—(Co/Ga)6	2.571 (3)
(Co/Ga)3—(Co/Ga)8	2.417 (3)
(Co/Ga)3—(Co/Ga)5	2.509 (3)
(Co/Ga)3—(Co/Ga)7	2.581 (3)
(Co/Ga)4—(Co/Ga)6	2.4986 (14)
(Co/Ga)5—(Co/Ga)8	2.495 (2)
(Co/Ga)5—(Co/Ga)7	2.506 (2)
(Co/Ga)6—(Co/Ga)6	2.424 (5)
(Co/Ga)6—(Co/Ga)6	2.563 (5)
(Co/Ga)7—(Co/Ga)7	2.413 (4)
(Co/Ga)7—(Co/Ga)7	2.574 (4)
(Co/Ga)8—(Co/Ga)8	2.423 (4)
(Co/Ga)8—(Co/Ga)8	2.564 (4)

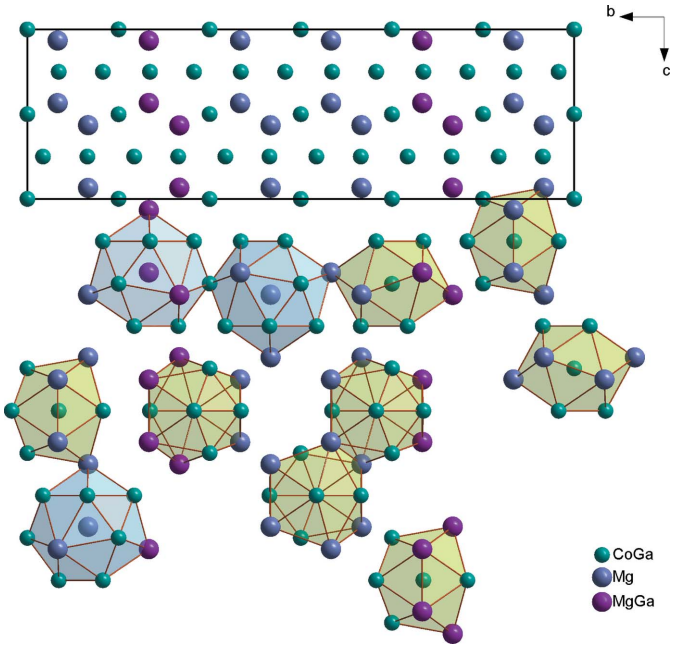

Figure 2
Phase **II** ($Mg_{0.74}CoGa_{0.52}$) unit cell and coordination polyhedra for each atomic position.

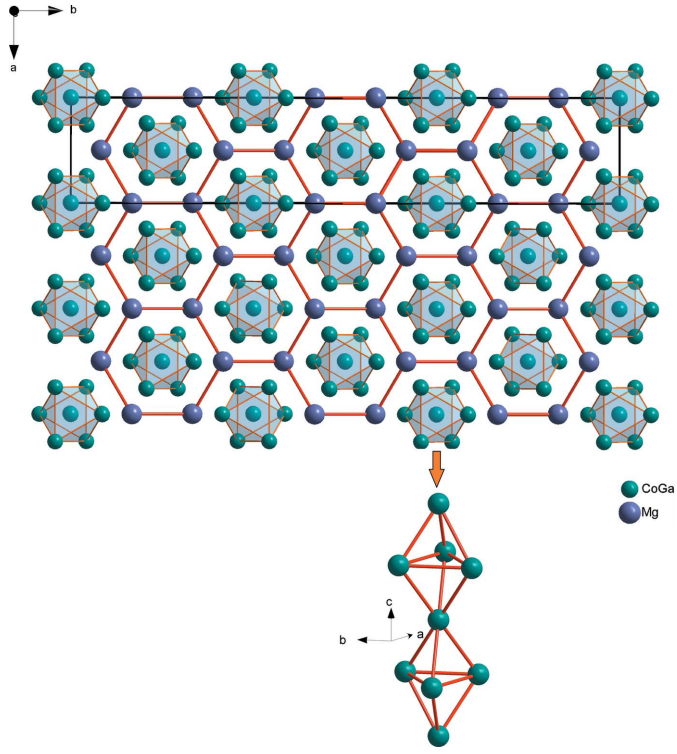

Figure 3
The 6_3-corrugated networks formed from magnesium atoms and Co/Ga-based tetrahedra packing in phase **II** ($Mg_{0.74}CoGa_{0.52}$) phase.

alism (Bärnighausen, 1980) (Fig. 4). In the first step, an orthorhombic URe_2 (*Cmcm*) phase can be received from $MgZn_2$ ($P6_3/mmc$) hexagonal phase via a *translationengleiche* symmetry reduction of index 3 (t3). Due to the symmetry reduction, the splitting of the 6*h* subcell site to 8*g* and 4*c* is observed. In the second step, the structure of phase **II** derives from an orthorhombic URe_2 via *klassengleiche* subgroups (a, 3b, c).

The structure of trigonal phase **III** is strongly disordered, as is shown by the presence of adjacent atomic sites which cannot be occupied simultaneously and split positions are observed (Tables 8, 9 and 10). Therefore, two subcells (A and B) can be selected, in a ratio of 9:1 (Fig. 5). Subcell A contains Mg, Co1, and Co2 atoms, but does not contain Ga1 or Ga2. The magnesium atom fully occupies the 6*c* site, and Co1 and Co2 occupy the 3*a* and 9*d* sites, respectively. The Mg_6Co_{12} (for $Z = 1$) or $MgCo_2$ (for $Z = 6$) composition was consequently obtained. Subcell A is closely related to $MgZn_2$-type. Similar to the parent structure, the coordination polyhedra for Mg in this subcell is a 16-vertex FK polyhedron. For the Co1 and Co2 atoms the coordination polyhedron is an icosahedron. The cobalt atoms in subcell A form the same Kagomé nets as Zn atoms in parent $MgZn_2$-type. Subcell B contains Co1, Ga1, and Ga2 atoms, but does not contain Mg or Co2 atoms. The cobalt atom fully occupies the 3*c* site, Ga1 partially occupies the 18*h* site, and Ga2 fully occupies the 6*a* site. For Co1 and Ga2 atoms the coordination polyhedron is a typical icosahedron and their deformed analog, respectively. The coordination polyhedron for the Ga1 atom is a distorted 15-vertex FK cage. The composition of subcell B can be described as Co_3Ga_{15} (for $Z = 1$) or $CoGa_5$ (for $Z = 3$). This hypothetically existing $CoGa_5$ motif of structure has no close analogs among known structural types.

Generally, in binary Lps, the ability to substitute transition metal atoms (Co, Ni, Cu, *etc.*) by *p*-block elements (Al, Ga, *etc.*) leads to the change of valence electron concentration (VEC) and results in the formation of disordered ternary Laves phases or their derivatives. The class of Laves Mg-based phases has many representatives, some of which, namely

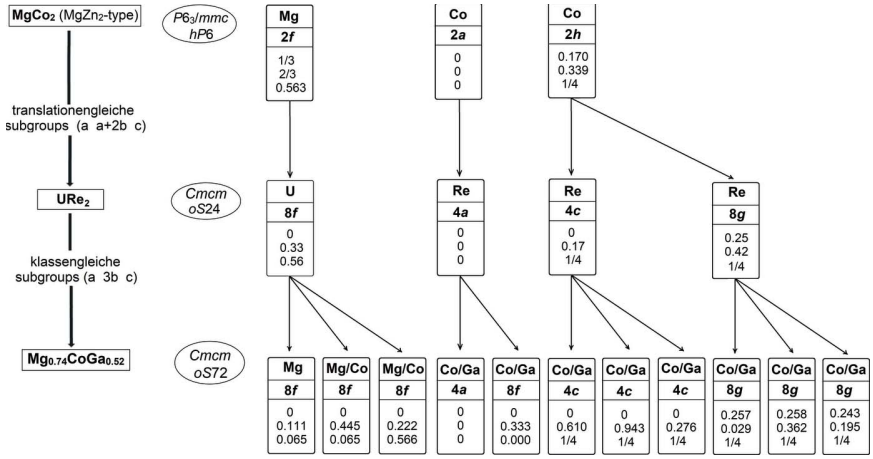

Figure 4
Group–subgroup scheme based on the Bärnighausen formalism for $MgCo_2$, URe_2 and phase **II** ($Mg_{0.74}CoGa_{0.52}$).

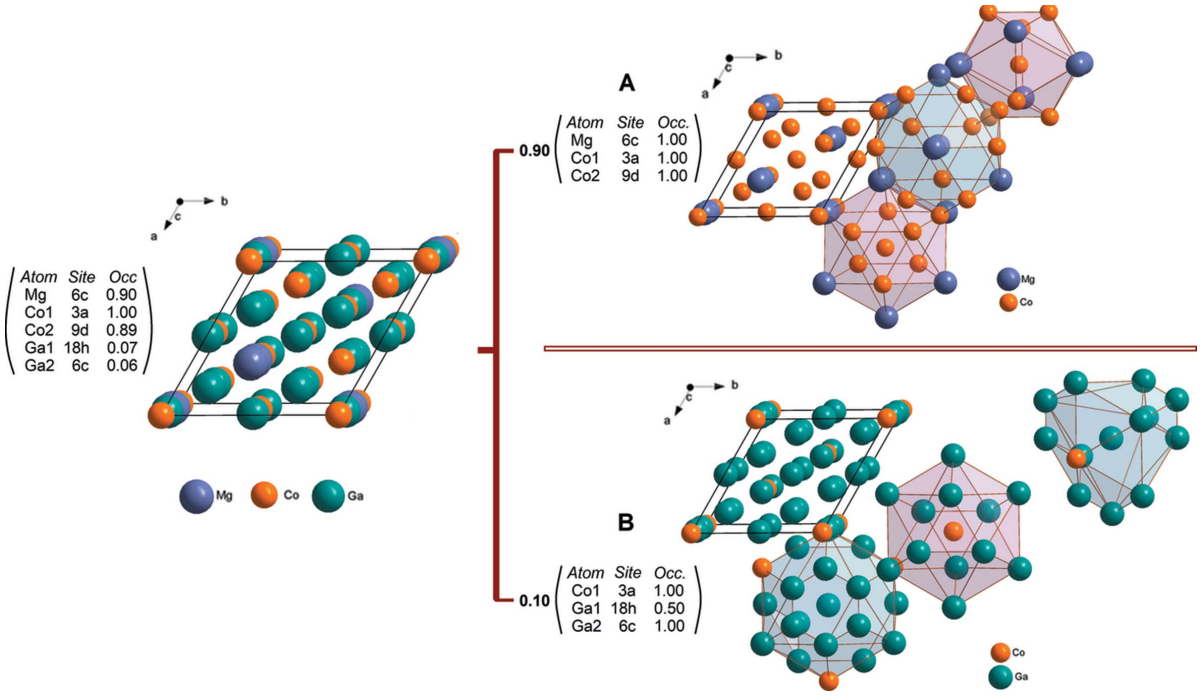

Figure 5
Subcells A and B of phase **III** ($Mg_{0.49}CoGa_{0.15}$) showing the coordination polyhedra of the atoms. The distributions of the atoms in the Wyckoff sites of the average cell and provided subcells are given.

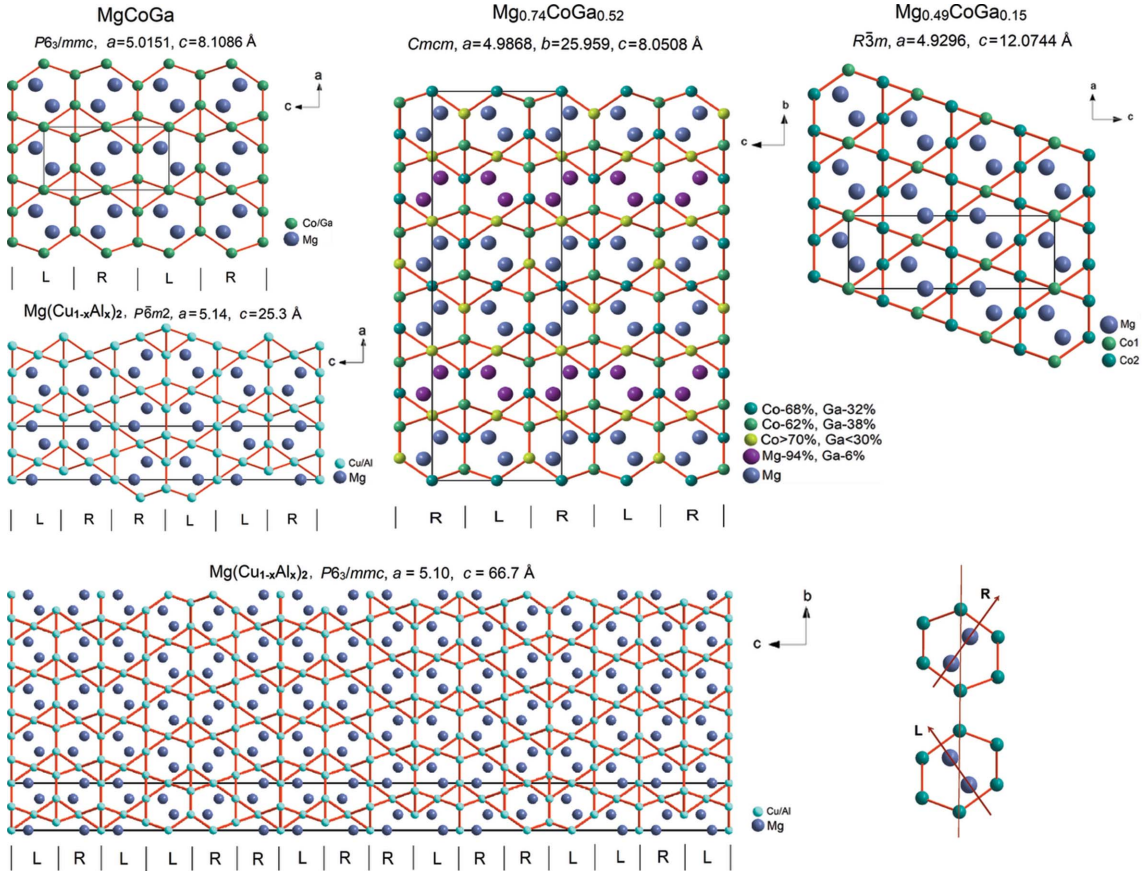

Figure 6
Atomic nets in Laves phases of Mg–Co–Ga and Mg–Cu–Al systems with filling of the hexagonal channels by Mg atoms. Bonds between Mg atoms in the channels can be tilted either to the right (R) or to the left (L) from the corresponding crystallographic axis.

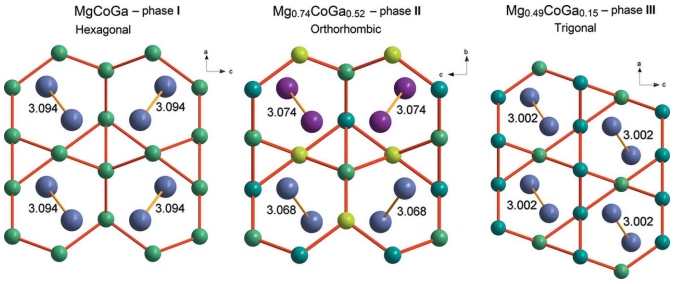

Figure 7
Changes in the Mg–Mg interatomic distances (Å) of the Mg–Co–Ga Laves phases in the selected structural fragment.

$MgZn_2$, $MgNi_2$ and $MgCu_2$, are the archetypes of Lp. Considering ternary systems, in the Mg–Ni–Ga system structural transitions of Laves phases with change of VEC is caused by substitution of Ni by Ga observed in the 33% Mg section (Pavlyuk *et al.*, 2022*a*). In binary Laves phase $MgNi_2$ (hexagonal, $P6_3/mmc$, *hP*24), the gradual substitution of Ni atoms by Ga leads to the formation of $MgNi_{1.6}Ga_{0.4}$ ($MgCu_2$ type), $MgNi_{1.25}Ga_{0.75}$ ($MgZn_2$ type), and $MgNi_{0.5}Ga_{1.5}$ (or Mg_2NiGa_3, orthorhombic derivative of the $MgZn_2$ type) ternary Lp phases.

The compositional heterogeneity of substituted elements in the crystal lattice nodes is the reason why the structures formed in this way can be described in relation to the parent structure as enlarged unit cells with reduced symmetry. In addition to the above-described **I**–**III** structures from the Mg–Co–Ga system, a similar one was previously observed in the Mg–Cu–Al system. The structure of equiatomic MgCuAl Laves phase is trigonal ($R\bar{3}m$, *hR*54) (Komura, 1962). The increase of copper content up to the composition $MgCu_{1.08}Al_{0.92}$ causes the transformation of the trigonal structure into the hexagonal phase with Pearson symbol of *hP*96 ($P6_3/mmc$) or *hP*36 ($P\bar{6}m2$) (Komura & Kitano, 1977). In the structure of all Lp phases from Mg–Co–Ga and Mg–Cu–Al systems, the transition metals (Ni and Cu) and *p*-elements (Al and Ga) do form tetrahedra-based 3-D nets with formation of hexagonal channels which are filled with Mg atoms. In these channels bonds between magnesium atoms can be tilted either to the right (R) or to the left (L) from the corresponding crystallographic axis. The Mg filling of the hexagonal channels for Lps of the Mg–Co–Ga and Mg–Cu–Al systems is shown in Fig. 6. The analysis of interatomic distances indicates that the atomic distances do decrease between magnesium atoms during the transition from the hexagonal to the rhombic and trigonal structure, which indicates compaction of the structural derivatives of the hexagonal Lp (Fig. 7).

Analysis of distances (Tables 4, 7 and 10) also shows some shortening of Ga-Ga distances. In the structure of elemental gallium, the Ga–Ga distance is 2.484 Å (Sharma & Donohue, 1962). In structures **I**, **II** and **III**, the shortest Ga–Ga distances are 2.456 Å, 2.417 Å and 2.330 Å, respectively. The maximum reduction of Ga–Ga distance observed for phase **III** does not exceed 6% compared to the structure of elementary Ga. This shortening of Ga–Ga distances results from the appearance of an additional partial covalent interaction between these atoms. Nevertheless, the main bonds are a metallic type of bond, as indicated by the remaining distances, which are typical for magnesium-containing intermetallics with transition and other metals (Solokha *et al.*, 2009; Shtender *et al.*, 2017; Pavlyuk *et al.*, 2020*a*,*b*).

Table 8
Fractional atomic coordinates and isotropic or equivalent isotropic displacement parameters (Å^2) for phase **III** ($Mg_{0.49}CoGa_{0.15}$).

Atoms	Wyckoff site	*x*	*y*	*z*	U_{iso}*/U_{eq}	Occ.
Co1	3*a*	0	0	0	0.0117 (6)	1.000
Co2	9*d*	$\frac{5}{6}$	$\frac{2}{3}$	$\frac{1}{6}$	0.0065 (5)	0.89 (2)
Mg1	6*c*	$\frac{1}{3}$	$\frac{2}{3}$	0.0402 (4)	0.0095 (10)	0.90 (3)
Ga1	18*h*	0.669 (2)	0.8343 (10)	0.1673 (9)	0.008 (2)*	0.067 (5)
Ga2	6*c*	$\frac{1}{3}$	$\frac{2}{3}$	−0.0127 (16)	0.008 (2)*	0.072 (4)

Table 9
Atomic displacement parameters (Å^2) for **III** ($Mg_{0.49}CoGa_{0.15}$).

Atoms	U_{11}	U_{22}	U_{33}	U_{12}	U_{13}	U_{23}
Co1	0.0093 (8)	0.0093 (8)	0.0166 (12)	0.0046 (4)	0.000	0.000
Co2	0.0057 (6)	0.0047 (8)	0.0086 (8)	0.0023 (4)	0.0002 (2)	0.0004 (4)
Mg1	0.0075 (13)	0.0075 (13)	0.014 (2)	0.0037 (6)	0.000	0.000

Table 10
Geometric parameters (Å) for **III** ($Mg_{0.49}CoGa_{0.15}$).

Co1—Co2	2.4650 (1)
Co1—Co2	2.4645 (1)
Co1—Ga1	2.466 (10)
Co2—Ga2	2.341 (16)
Co2—Co2	2.4646 (1)
Co2—Co2	2.4651 (1)
Mg1—Ga1	2.864 (11)
Mg1—Ga2	2.865 (3)
Ga1—Ga2	2.330 (17)
Ga1—Ga1	2.451 (15)
Ga1—Co1	2.466 (10)
Ga1—Ga1	2.479 (15)
Ga2—Ga1	2.330 (17)
Ga2—Ga1	2.59 (2)
Ga2—Ga1	2.602 (18)

4. General conclusion

Three new phases from the Mg–Co–Ga system, MgCoGa, $Mg_{0.74}CoGa_{0.52}$ and $Mg_{0.49}CoGa_{0.15}$, were synthesized. Their crystal structures were determined using single crystal X-ray diffraction. The chemical compositions were confirmed by EDS/WDS dispersive spectrometry and density measurements. The crystal structures of all phases were successfully solved by direct methods. These structures are related to known Laves phases, especially binary $MgZn_2$ and ternary Mg_2MnGa_3 and $Mg(Cu_{1-x}Al_x)_2$. Hexagonal MgCoGa crystallizes as a disordered phase with parent $MgZn_2$ structure type. The orthorhombic structure of $Mg_{0.74}CoGa_{0.52}$ is a distortion variant of both $MgZn_2$ and URe_2 phases and can be derived from them by using group–subgroup transformation schemes of the Bärnighausen formalism. The trigonal $Mg_{0.49}CoGa_{0.15}$ phase is described as strongly disordered composite structure.

In the $Mg_{0.49}CoGa_{0.15}$ phase, two subcells (A and B) were found, with subcell A to subcell B ratio of 9:1. Subcell A corresponds to the $MgZn_2$-type. In binary Laves phases, the ability to substitute transition metal atoms (Co, Ni, Cu, *etc*.) by *p*-block elements (Al, Ga, *etc*.) leads to the change of valence electron concentration and results in the formation of disordered ternary Laves phases or their derivatives.

Funding information

The following funding is gratefully acknowledged: Narodowe Centrum Nauki (grant No. 2017/25/B/ST8/02179); Deutscher Akademischer Austauschdienst (scholarship No. 91774331); Simons Foundation (award No. 1037973).

References

Bououdina, M., Grant, D. & Walker, G. (2006). *Int. J. Hydrogen Energ.* **31**, 177 182.
Bärnighausen, H. (1980). *MATCH Commun. Math. Comput. Chem.* **9**, 139 175.
Brandenburg, K. (2006). *DIAMOND*. Crystal Impact GbR, Bonn, Germany.
Horechyy, A. I., Pavlyuk, V. V. & Bodak, O. I. (1999). *Pol. J. Chem.* **73**, 1681 1685.
Komura, Y. (1962). *Acta Cryst.* **15**, 770 778.
Komura, Y. & Kitano, Y. (1977). *Acta Cryst.* B**33**, 2496 2501.
Komura, Y., Nakaue, A. & Mitarai, M. (1972). *Acta Cryst.* B**28**, 727 732.
Komura, Y. & Tokunaga, K. (1980). *Acta Cryst.* B**36**, 1548 1554.
Laves, F. & Witte, H. (1935). *Metallwirtsch.* **14**, 645 649.
Massalski, T. B., Murray, J. L., Bennett, L. H. & Baker, H. (1986). *Binary Alloy Phase Diagrams*. Materials Park, Ohio: ASM.
Okamoto, H. (2013). *J. Phase Equilib. Diffus.* **34**, 148.
Oxford Diffraction (2008). *CrysAlis CCD* and *CrysAlis RED*. Oxford Diffraction Ltd, Abingdon, England.
Paufler, P. (2011). *Intermetallics*, **19**, 599 612.
Pavlyuk, N., Chumak, I., Pavlyuk, V., Ehrenberg, H., Indris, S., Hlukhyy, V. & Pöttgen, R. (2022*b*). *Z. Naturforsch. B*, **77**, 727 733.
Pavlyuk, N., Dmytriv, G., Pavlyuk, V., Chumak, I., Indris, S. & Ehrenberg, H. (2022*a*). *J. Phase Equilib. Diffus.* **43**, 458 470.
Pavlyuk, N., Dmytriv, G., Pavlyuk, V., Rożdżyńska-Kiełbik, B., Gil, A., Chumak, I. & Ehrenberg, H. (2020*b*). *Z. Kristallogr. Cryst. Mater.* **235**, 513 521.
Pavlyuk, N., Dmytriv, G., Pavlyuk, V., Rozdzynska-Kielbik, B., Nitek, W., Lasocha, W., Chumak, I. & Ehrenberg, H. (2020*a*). *Acta Cryst.* C**76**, 541 546.
Pavlyuk, V., Marciniak, B. & Różycka-Sokołowska, E. (2012). *Intermetallics*, **20**, 8 15.
Pavlyuk, V., Solokha, P., Dmytriv, G., Marciniak, B. & Paul-Boncour, V. (2007). *Acta Cryst.* E**63**, i161.
Sakintuna, B., Lamaridarkrim, F. & Hirscher, M. (2007). *Int. J. Hydrogen Energ.* **32**, 1121 1140.
Sharma, B. D. & Donohue, J. (1962). *Z. Kristallogr.* **117**, 293 300.
Sheldrick, G. M. (2008). *Acta Cryst.* A**64**, 112 122.
Sheldrick, G. M. (2015). *Acta Cryst.* C**71**, 3 8.
Shtender, V., Zelinska, O. Ya., Pavlyuk, V. V., Denys, R. V., Paul-Boncour, V., Zavaliy, I. Yu., Marciniak, B. & Różycka-Sokołowska, E. (2017). *Intermetallics*, **87**, 61 69.
Shtender, V. V., Denys, R. V., Zavaliy, I. Yu., Zelinska, O. Y., Paul-Boncour, V. & Pavlyuk, V. V. (2015). *J. Solid State Chem.* **232**, 228 351.
Solokha, P., De Negri, S., Pavlyuk, V. & Saccone, A. (2009). *Inorg. Chem.* **48**, 11586 11593.
Stein, F. & Leineweber, A. (2021). *J. Mater. Sci.* **56**, 5321 5427.
Teslyuk, M. Y. & Markiv, V. Y. (1962). *Sov. Phys. Crystallogr.* **7**, 103 104.